Supplementary Information

A strain-modulated CoRu alloy supported on nitrogen-doped carbon nanospheres for defect-driven industrial chlorine evolution electrocatalysis

Bo Zhang [a,1], Qiqi Zhang [a,1], Ru Xiao [a], Xiaoxuan Min [a], Huiqi Jia [a], Kang Liu [a], Ying Deng [a,*], Zhenyu Xiao [a,*], Lei Wang [a,*]

[a] Key Laboratory of Eco-chemical Engineering, Ministry of Education, International Science and Technology Cooperation Base of Eco-chemical Engineering and Green Manufacturing, College of Chemistry and Molecular Engineering, Qingdao University of Science and Technology, Qingdao 266042, P. R. China.

E-mail: dengyingchem@163.com; inorgxiaozhenyu@163.com; inorchemwl@126.com.

[1] These authors contributed equally.

Supplementary electrochemical tests

The overpotential (η) is computed using the formula: $\eta = E_{RHE} - E_{CER}$. In addition, the E_{CER}^{0} of the CER is sensitive to temperature, implying that

$$E_{CER}^{0} = \left(1.358\,V + \frac{RT\,ln10}{F}\,pH\right) - \left(0.001248\,\frac{\partial E}{\partial T}\right)(T - 298.15K)\ vs\ RHE$$

where R is the gas constant (8.314 J K^{-1} mol^{-1}), T is temperature in Kelvin (K), and F is the Faraday constant (96,485.3 C mol^{-1}).

The equilibrium potential of the CER (E_{CER}) can be calculated using the Nernst equation, incorporating chloride ion activity and chlorine gas partial pressure:

$$E_{CER}\,(T, \alpha(Cl_2), \alpha(Cl^-))\ \text{vs RHE} = E_{CER}^{0} - \left(\frac{RT}{F}\right) ln\alpha(Cl^-) + \left(\frac{RT}{2F}\right) ln\alpha(Cl_2)$$

where $\alpha(Cl_2)$ is 0.01, corresponding to the partial pressure of evolving Cl_2 under an Ar atmosphere, and $\alpha(Cl^-)$ is defined by the experimental conditions (e.g., $\alpha(Cl^-)$ = 5.0 for 5.0 M NaCl).

Supplementary Figures 1 to 20

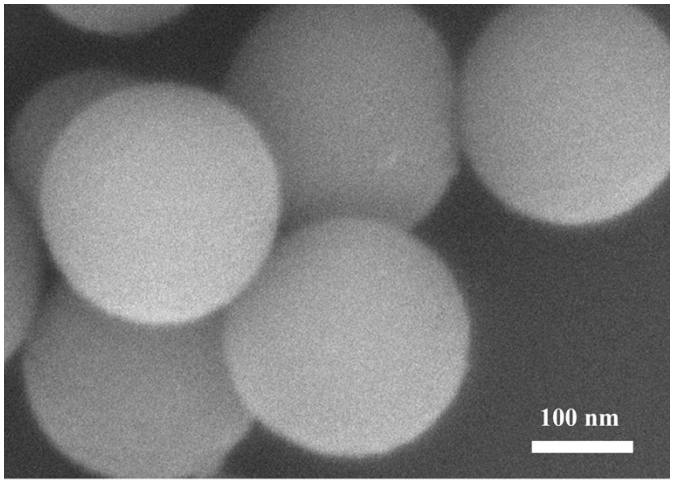

Figure S1. The SEM image of PDA NSs.

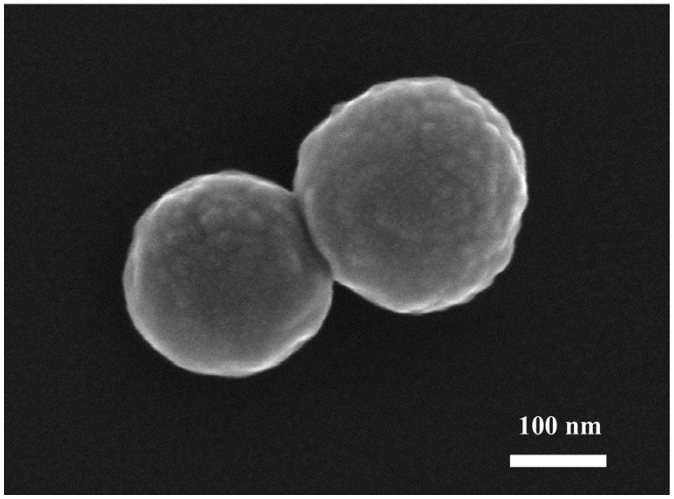

Figure S2. The SEM image of CoRu@PDA.

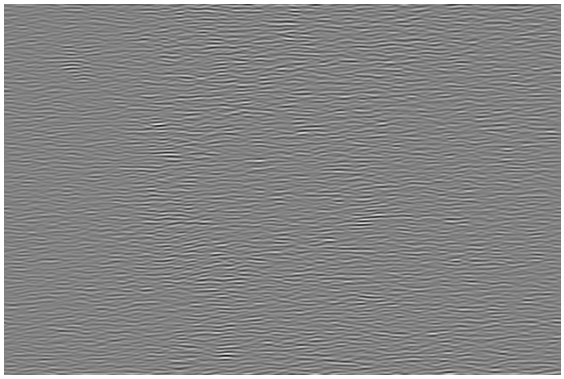

Figure S3. Geometric Phase Analysis strain of CoRu@CN.

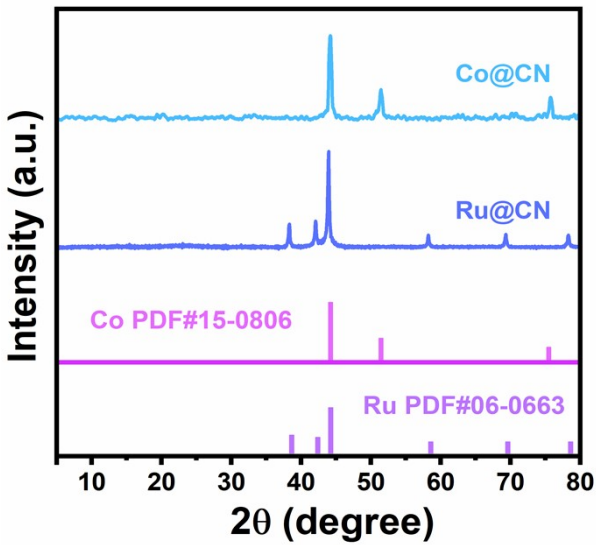

Figure S4. XRD pattern of Co@CN and Ru@CN.

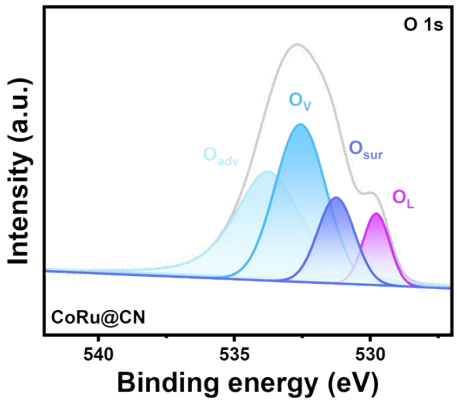

Figure S5. O 1s XPS spectra of CoRu@CN.

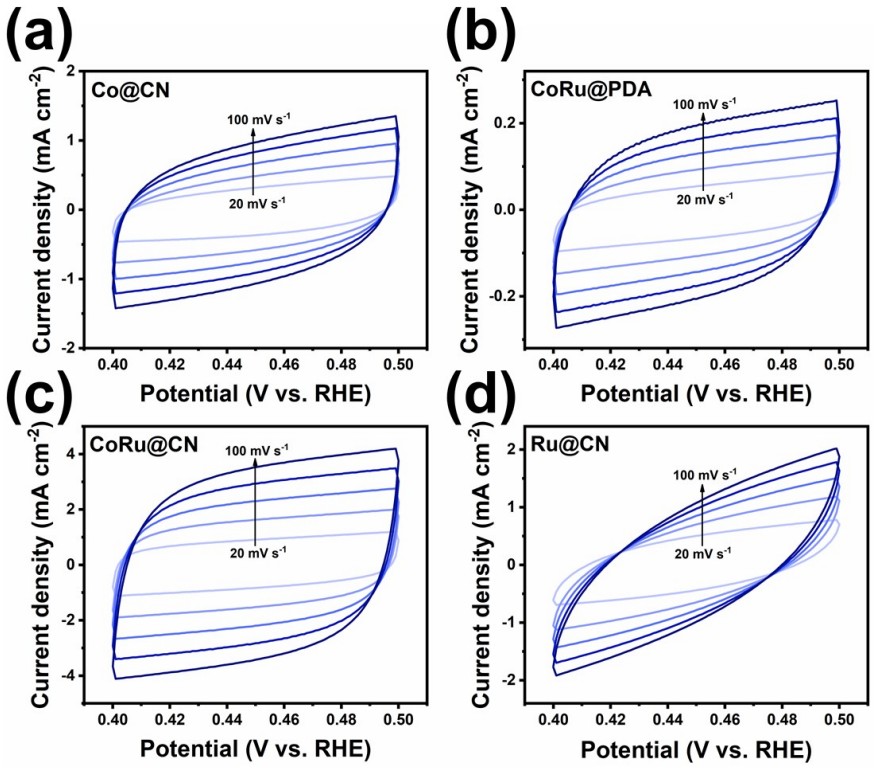

Figure S6. Cyclic voltammetry curves of the (a) Co@CN, (b) CoRu@PDA , (c) CoRu@CN and (d) Ru@CN under different scan rate in a region of 0.4 to 0.5 V vs. RHE.

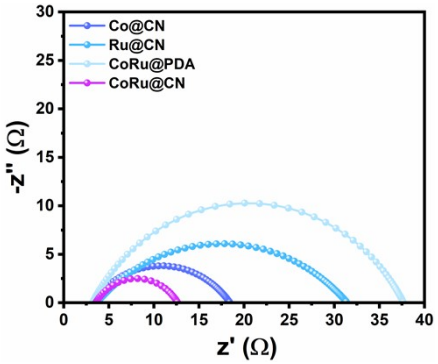

Figure S7. EIS of Co@CN, Ru@CN, CoRu@PDA, and CoRu@CN.

Figure S8. Post-stability SEM.

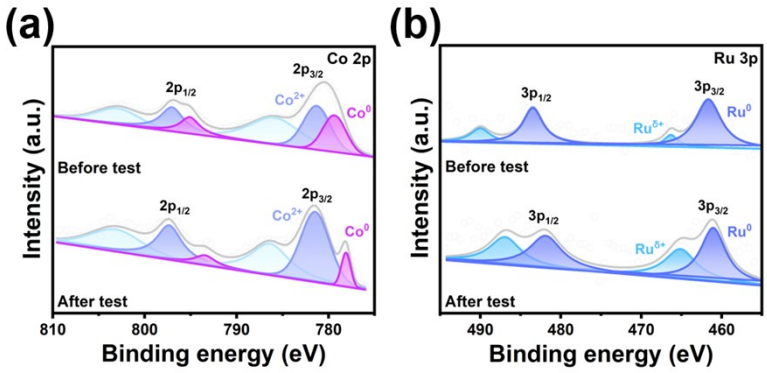

Figure S9. Post-stability XPS.

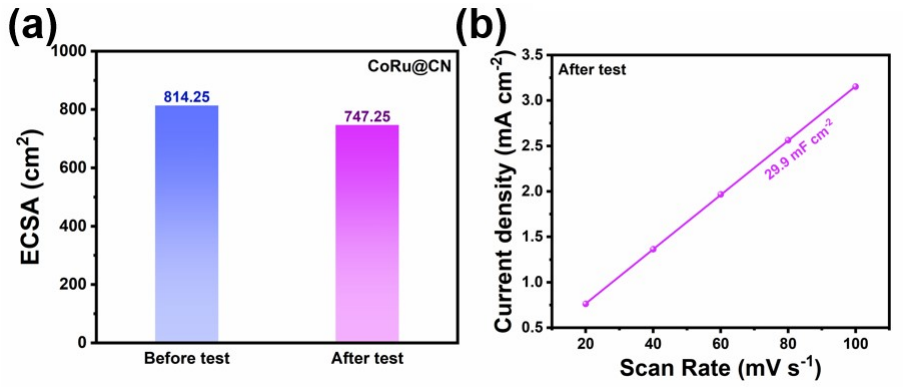

Figure S10. Comparison of ECSA of CoRu@CN before and after stability test.

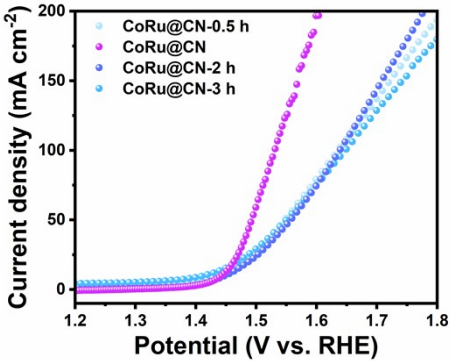

Figure S11. LSV curves of CoRu@CN with different durations.

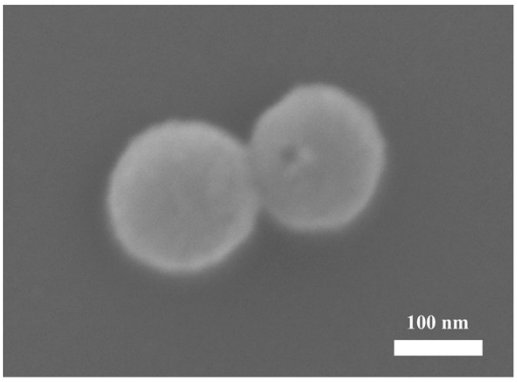

Figure S12. The SEM image of CoRu@CN-3h.

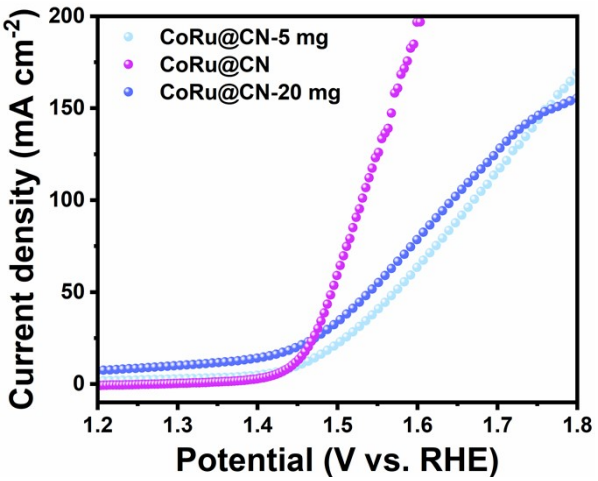

Figure S13. LSV curves of CoRu@CN with different Ru doping amount.

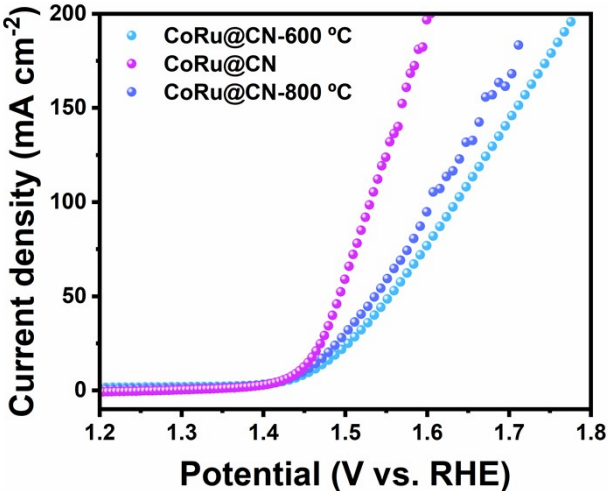

Figure S14. LSV curves of CoRu@CN with an oxidation rate of 2℃·min^{-1} and different oxidation temperatures.

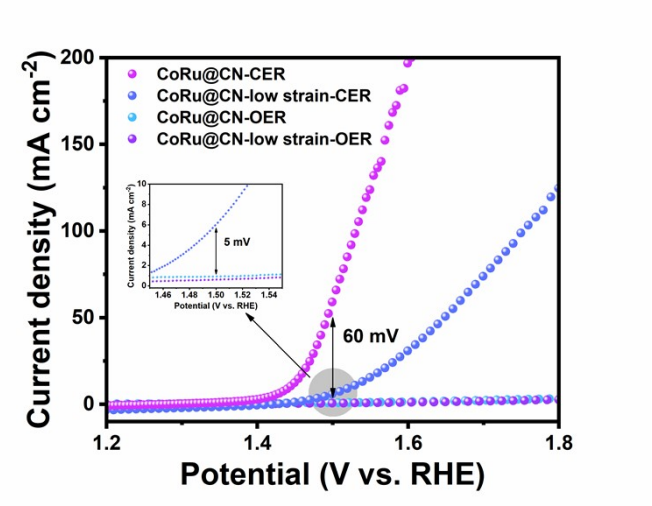

Figure S15. The LSV curves of OER and CER for CoRu@CN and CoRu@CN-low strains.

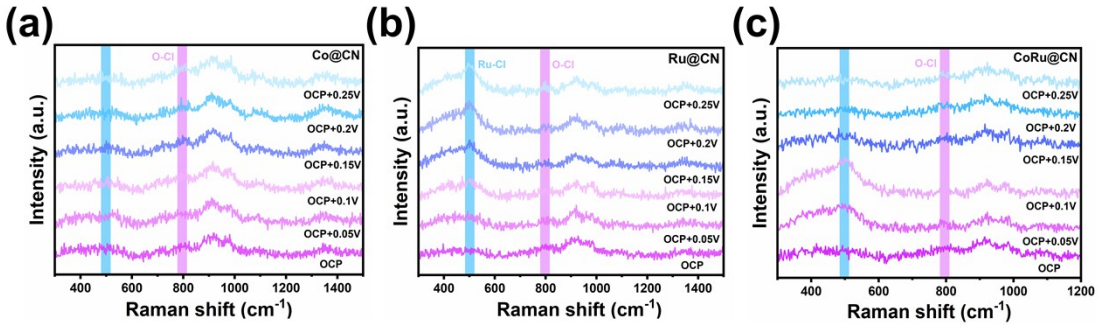

Figure S16. In situ Raman spectra of (a) Co@CN, (b) Ru@CN and (c) CoRu@CN recorded in a solution of H_2SO_4 with pH = 2 5 M NaCl from OCP to OCP + 0.25 V.

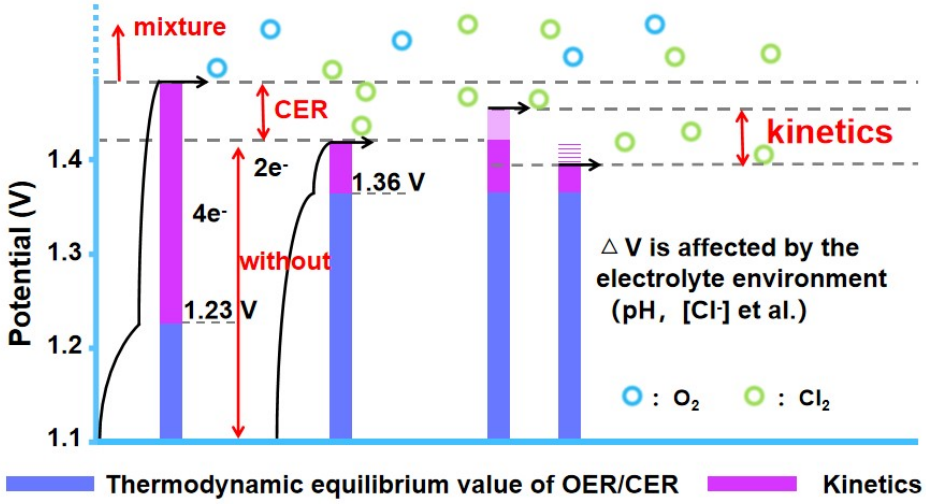

Figure S17. The kinetic potential is affected by the electrolyte environment. Schematic diagram illustrating the potential composition and product selectivity mechanism of the OER and the CER. The blue area represents the thermodynamic equilibrium potential of OER/CER, while the purple area represents the potential contribution from the kinetic process. The hollow blue circle and green circle correspond to the actual potential changes of O_2 and Cl_2 generation, respectively. The red annotation indicates the number of electron transfers in the reaction, the trend of product selectivity dominated by kinetics, and also shows the regulatory effect of the electrolyte environment (pH, Cl^- concentration, etc.) on the potential difference (△V) between OER and CER.

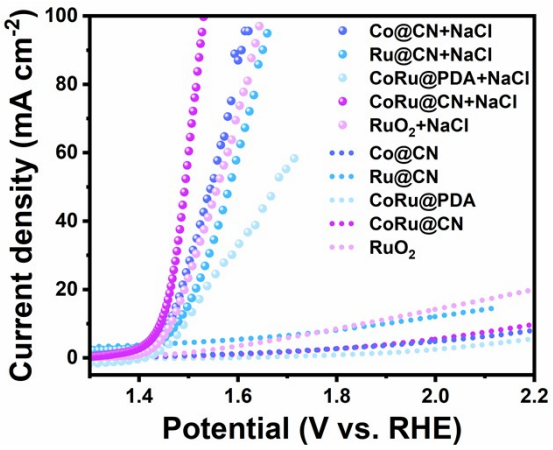

Figure S18. LSV curves of OER and CER (solid line is in H_2SO_4 with pH = 2 + 5 M NaCl; dashed line is in H_2SO_4 with pH = 2).

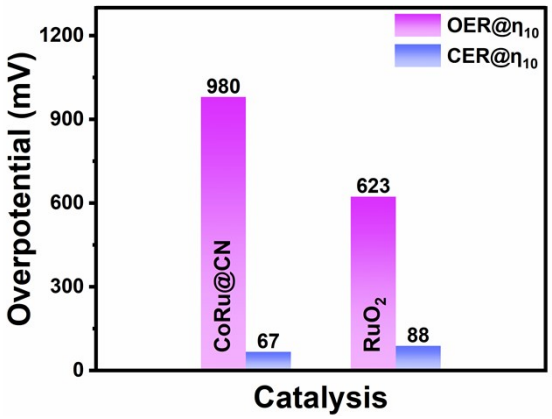

Figure S19. The overpotentials of CoRu@CN and RuO_2 at 10 mA·cm^{-2} about CER and OER processes, respectively.

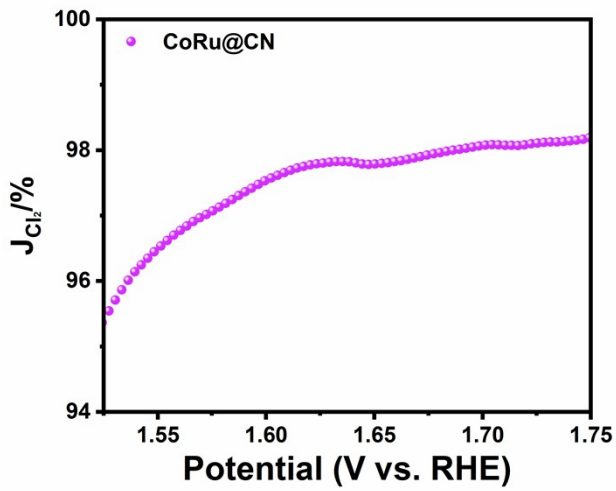

Figure S20. Current density percentage of Cl_2 selectivity of CoRu@CN in 5.0 M NaCl (pH = 2).

Supplementary Tables 1 to 3

Table 1. Detailed structural information of CoRu@CN derived from Rietveld Refinement.

Lattice type = F	Space group = F m -3 m	Space group number = 225
R = 1.02%	R_{wp} = 1.28%	R - bkg = 1.50%
R_{wmin} = 1.40%	GOF = 0.91	a(Å) = 3.5541
b(Å) = 3.5541	c(Å) = 3.5541	V(Å^3) = 44.893

Table 2. Comparison of catalytic activity with reported catalysts in the chlorine evolution reaction.

Catalyst	Solution	Overpotential (mV)		Ref.
CoRu@CN	5 M NaCl (pH = 2)	η_{10} = 67	η_{100} = 154	This work
$(CoZn)_2V_2O_8$@C	4 M NaCl (pH =0.5)	η_{10} = 69	η_{50} = 173	1
$Ag_{0.15}Ru_{0.85}O_2$	5.0 M NaCl (pH = 2)	η_{10} = 105		2
$Ti_{0.35}V_{0.35}Sn_{0.25}Sb_{0.05}$-oxide	5 M NaCl + 0.01 M HCl（pH = 2）	η_{10} = 138	η_{100} = 208	3
1% Ru@Ti_4O_7	5.0 M NaCl (pH = 1)	η_{10} = 96.5		4
Ru-Ni-Sb-SnO_2/ND-2	1.0 M NaCl (pH = 1)	η_{10} = 130		5
Ru-Ir-Ce-Ni-Sb-SnO_2	0.3 M NaCl	η_{10} = 80	η_{100} = 124	6

(pH = 6)

Catalyst	Solution	Overpotential (mV)		Ref.
HPC-0.05	4 M NaCl (pH = 2)	η_{10} = 94	η_{100} = 269	7
$IrB_{1.15}$	4 M NaCl (pH = 2)	η_{10} = 75		8
Cu_1@FeN@TiFelt	4 M NaCl (pH = 2)	η_{10} = 238	η_{100} = 432	9
Ni_1/aniCNT	0.1 M $HClO_4$ + 1.0 M NaCl (pH = 1)	η_{10} = 70		10
$Ru_{0.09}Co_{2.91}O_4$	0.6 M NaCl (pH = 7)	η_{10} = 70	η_{100} = 120	11

Table 3. The CER stability at a current density of 10 mA cm^{-2} is compared against the stability of benchmark catalysts documented in prior studies.

Catalyst	Solution	Current density (mA cm^{-2})	Stability (h)	Ref.
CoRu@CN	5 M NaCl (pH = 2)	10	100	This work
m-CNP/CC	2 M NaCl (pH = 6)	10	24	[12]
CC/350	0.6 M NaCl (pH = 6)	10	60	[13]
$Na_{0.7}CoO_2$	HCl or HNO_3 electrolyte (pH = 2)	10	20	[14]
$IrB_{1.15}$	4 M NaCl (pH = 2)	<10	90	[8]
$RuTi_2$/MXene@C C	4 M NaCl (pH = 2)	10	80	[15]
Ir_2-ONC	0.1 M $HClO_4$ + 4 M NaCl.	10	20	[16]

$Ni_{79}Mo_{21}@IrO_2$	4 M NaCl (pH = 1)	10	10	[17]
Ru_1 TiO_x/Ti	4 M NaCl (pH = 2)	10	24	[18]

Catalyst	**Solution**	**Current density (mA cm^{-2})**	**Stability (h)**	**Ref.**
Pt_1/CNT	0.1 M $HClO_4$ + 1 M NaCl.	＜10	12	[19]
PtNP/CNT	0.1 M $HClO_4$ + 1 M NaCl.	＜10	12	[19]
Pt-2	0.1 M $HClO_4$ + 1 M NaCl.	＜10	24	[20]

References

1 L. Liu, J. Xu, X. Yang, C. Xu, Y. Bai, Y. Ma, R. Wang and W. Fu, In situ evolved high-valence Co active sites enable highly efficient and stable chlorine evolution reaction, *J. Colloid Interface Sci.*, 2025, **682**, 528-539.

2 Y. Cheng, P. Meng, L. Li, L. Zhong, C. Yuan, J. Chen and Q. Liang, Boosting selective chlorine evolution reaction: Impact of Ag doping in RuO_2 electrocatalysts, *J. Colloid Interface Sci.*, 2025, **685**, 97-106.

3 M. Mirzaei Alavijeh, S. Habibzadeh, K. Roohi, F. Keivanimehr, L. Naji and M.R. Ganjali, A selective and efficient precious metal-free electrocatalyst for chlorine evolution reaction: An experimental and computational study, *Chem. Eng. J.*, 2021, **421**, 127785.

4 J. Lai, R. Zeng, X. Bian, W. Leng, C. Yang, L. Yang, W. Li, G. Wang, G. He and S. Lv, Ultralow Ru nanoparticle-loaded Ti_4O_7 anodes for efficient chlorine evolution and sustainable farm odor spray wastewater treatment, *Applied Surface Science*, 2025, **695**, 162891.

5 J. Cai, J. Si, J. Liu, Y. Xue, Z. Xu, Y. Wang, Y. Wang, Y. Ding, H. Cao, Y. Cao, S. Wang, X. Zhong and J. Wang, Highly active multicomponent metal oxides/nanodiamond hybrid for enhanced electrochemical ozone production and chlorine evolution reaction, *Appl. Catal. B-Environ.*, 2025, **366**, 125015.

6 M. Xue, J. Zhao, X. Yu, L. Ding, X. Wang, J. Liu, H. Shi, Y. Xue, Z. Yao, X. Zhong and J. Wang, Facilitating electrochemical ozone production and chlorine evolution reaction by synergistic effect of multicomponent metal oxides, *Adv. Funct. Mater.*, 2023, **34**, 2308567.

7 H. Qu, B. Li, Y. Ma, Z. Xiao, Z. Lv, Z. Li, W. Li and L. Wang, Defect-enriched hollow porous carbon nanocages enable highly efficient chlorine evolution reaction, *Adv. Mater.*, 2023, **35**, e2301359.

8 T. Liu, Z. Chen, S. Liu, P. Wang, Z. Pu, G. Zhang and S. Sun, Ultrafast synthesis of $IrB_{1.15}$ nanocrystals for efficient chlorine and hydrogen evolution reactions in saline water, *Angew. Chem.-Int. Edit*, 2024, **64**, e202414021.

9 A. Badreldin, E. Youssef, A. El-Ghenymy, M.Z. Ansari, K. Elsaid, A. Abdala and A. Abdel-Wahab, Harnessing iron nitride matrices through incorporated Cu-based moieties for chlorine evolution reaction, *ACS Appl. Energy Mater.*, 2024, **7**, 9156-9167.

10 J. Kim, T. Lim, D. Hernandez-Castillo, J.S. Lim, J. Park, D. Kim, J. Kim, J. Ryu, Y.J. Sa, J.H. Lee, Y.J. Hwang, H.R. Moon, K.S. Exner and S.H. Joo, Identification of Ni-N_4 active sites in atomically dispersed Ni catalysts for efficient chlorine evolution reaction, *J. Am. Chem. Soc.*, 2025, **147**, 27664-27675.

11 W.I. Choi, S. Choi, M. Balamurugan, S. Park, K.H. Cho, H. Seo, H. Ha and K.T. Nam, Ru-doped Co_3O_4 nanoparticles as efficient and stable electrocatalysts for the chlorine evolution reaction, *ACS Omega*, 2023, **8**, 35034-35043.

12 Y. Zhang, G. Qu, Y. Wang, Z. Li, J. Zhou, P. Ning and N. Ren, Advancing chlorine evolution reaction efficiency through magnetization-induced electron polarization

and surface PdO exposure on ferromagnetic CNP/CC electrodes, *Int. J. Hydrogen Energy*, 2025, **105**, 583-591.
13 X. Zhang, D. Wu, X. Liu, Y. Qiu, Z. Liu, H. Xie, J. Duan and B. Hou, Efficient electrocatalytic chlorine evolution under neutral seawater conditions enabled by highly dispersed Co_3O_4 catalysts on porous carbon, *Appl. Catal. B-Environ.*, 2023, **330**, 122594.
14 G. Chen, J. Yang, Z. Huang, L. Chen, W. Duan, T. Wang, X. Kong and H. Yang, Engineering the interlayer sodium density in layered sodium cobalt oxide for boosted chlorine evolution reaction, *Chin. Chem. Lett.*, 2025, **36**, 111662.
15 Y. Duan, L. Wei, C. Cai, J. Mi, F. Cao, J. Chen, X. Li, X. Pang, B. Li and L. Wang, RuO_2/TiO_2/MXene with multi-heterojunctions coating on carbon cloth for high-activity chlorine evolution reaction at large current densities, *Nano Res.*, 2024, **17**, 4764-4772.
16 Z. Yu, G. Xia, V.M. Diaconescu, L. Simonelli, A.P. LaGrow, Z. Tai, X. Xiang, D. Xiong and L. Liu, Atomically dispersed dinuclear iridium active sites for efficient and stable electrocatalytic chlorine evolution reaction, *Chem. Sci.*, 2024, **15**, 9216-9223.
17 Z. Lin, G. Song, Y. Yu, Y. Li, S. Feng, E. Shi, Y. Zhao, Z. Ren and Y. Zhu, NiMo@IrO_2 bifunctional electrocatalyst for efficient electrochemical hydrogen evolution and chlorine evolution reactions, *J. Electroanal. Chem.*, 2025, **978**,
18 Y. Yao, L. Zhao, J. Dai, J. Wang, C. Fang, G. Zhan, Q. Zheng, W. Hou and L. Zhang, Single atom Ru monolithic electrode for efficient chlorine evolution and nitrate reduction, *Angew. Chem.-Int. Edit*, 2022, **61**, e202208215.
19 T. Lim, G.Y. Jung, J.H. Kim, S.O. Park, J. Park, Y.T. Kim, S.J. Kang, H.Y. Jeong, S.K. Kwak and S.H. Joo, Atomically dispersed Pt-N_4 sites as efficient and selective electrocatalysts for the chlorine evolution reaction, *Nat. Commun.*, 2020, **11**, 412.
20 M. Ha, P. Thangavel, N.K. Dang, D.Y. Kim, S. Sultan, J.S. Lee and K.S. Kim, High-performing atomic electrocatalyst for chlorine evolution reaction, *Small*, 2023, **19**, e2300240.